



AIAA 2002-3411

Development of Micro Air Reconnaissance Vehicle as a Test Bed For Advanced Sensors and Electronics

Qamar A. Shams,¹ Thomas L. Vranas,¹ Robert L. Fox,¹ Theodore R. Kuhn,¹ John Ingham,¹ Michael J. Logan,¹ Kevin N. Barnes,¹ and Benjamin F. Guenther²

NASA Langley Research Center
Hampton, VA 23681-2199

**1st AIAA Unmanned Aerospace Vehicles, Systems, Technologies,
and Operations Technical Conference and Workshop**
20-23 May 2002 / Portsmouth, VA

For permission to copy or to republish, contact the copyright owner named on the first page.
For AIAA-held copyright, write to AIAA Permissions Department,
1801 Alexander Bell Drive, Suite 500, Reston, VA, 20191-4344.

DEVELOPMENT OF MICRO AIR RECONNAISSANCE VEHICLE AS A TEST BED FOR ADVANCED SENSORS AND ELECTRONICS

Qamar A. Shams, Thomas L. Vranas, Robert L. Fox, Theodore R. Kuhn,
John Ingham, Michael J. Logan, Kevin N. Barnes, and Benjamin F. Guenther
NASA Langley Research Center
Hampton, VA 23681

Abstract

This paper describes the development of a Micro/Mini Air Reconnaissance Vehicle for advanced sensors and electronics at NASA Langley Research Center over the last year. This vehicle is expected to have a total weight of less than four pounds, a design velocity of 40 mph, an endurance of 15-20 minutes, and a maximum range of 5km. The vehicle has wings that are simple to detach yet retain the correct alignment. The upper fuselage surface has a quick release hatch used to access the interior and also to mount the varying propulsion systems. The sensor suite developed for this vehicle consists of a pitot-static measurement system for determining air speed, an absolute pressure measurement for determining altitude, magnetic direction measurement, and three orthogonal gyros to determine body angular rates. Swarming GPS-guidance and in-flight maneuvering is discussed, as well as design and installation of some other advance sensors like MEMS microphones, infrared cameras, GPS, humidity sensors, and an ultrasonic sonar sensor. Also low cost, small size, high performance control and navigation system for the Micro Air Vehicle is discussed. At the end, laboratory characterization of different sensors, motors, propellers, and batteries will be discussed.

completed at NASA Langley with three objectives in mind.

1. UAVs will be fabricated using state-of-the-art lightweight, and high strength composites. New materials and methods have been researched for biomimetic and morphing characteristics.
2. The UAVs will provide a test bed for the smallest available Global Positioning System (GPS), MEMS sensors for measuring pressure, humidity, temperature, sound, altitude, vehicle stability, and magnetic disturbances. In addition, ultrasonic detection and an infrared camera are also being installed.
3. Design and control which facilitates the researcher's new research areas such as electric motors for flight, testing of batteries, low-level flight control algorithm design (control theory), and mode switching experiments, to high level swarming experiments.

Applications of Micro/ Mini Air Vehicles (MAVs) include visual reconnaissance, infrared detection, surveillance, biological or chemical agent sensing, communications link, and field damage assessment and awareness.¹ A few of the commercial applications for the unmanned UAVs are: search and rescue, patrol, air sampling, and surveillance. The one and a half-pound UAV (plus the weight of the servos, electronics and batteries) has been statically balanced and dynamically tested for short durations. The servos, electronics and batteries account for approximately two pounds, increasing the total weight of the UAV to nearly four pounds.

Introduction

Unmanned Air Vehicles (UAVs) are thrusting into the spotlight following the September 11, 01 terrorist incidents and during the subsequent anti-terrorist campaign under way in Afghanistan. The term unmanned may be a misnomer. There are few fully instrumented autonomous unmanned air vehicles in use today. In most cases humans through the use of ground-based commands have real time vehicle control of the UAVs flight parameters. As the supporting electronics technologies emerge, the human role will decrease to programming onboard control systems. Researchers and Technologists at NASA Langley Research Center have been involved in morphing and biomimetic research to learn how nature designs systems of staggering complexity yet provides robust, autonomous, and efficient solutions. In this regards, some preliminary design, fabrication, and analysis work has been

Advanced sensors and related electronics are other important areas for the design of UAVs. Over the last few years there has been rapid growth in Micro-electromechanical Systems (MEMS) technologies, onboard intelligent technologies, and smaller, faster, smarter wireless telemetry systems technologies that can reduce cycle time and total measurement and test process cost.^{2,3} The major attraction of MEMS technology is the order of magnitude reduction of the power and thermal requirements over existing

electronics components. In addition, the size requirements have also made them attractive for wind tunnel, field-deployable acoustics measurement systems, flight, and space applications. Recent advances in MEMS technology have made it possible to produce pressure, acceleration, humidity, and temperature sensors having masses in the milligram range or even lighter, and having the same sensitivity and accuracy of larger devices.

The Langley developed UAVs are quiet, have advanced manual control to allow operation by unskilled operators, and radio control electronics for the manually controlled elevons. The targeted payload of the unmanned UAVs is approximately one and one-half pounds, which will consist of MEMS sensors, miniature sized GPS, and an embedded reconfigurable computer and logic module for control and processing of data. These UAVs are made of lightweight and high-strength materials; they have a range of 5Km, and flight time of 15-20 minutes. A lightweight characterized system equipped with several sensors has been designed and is used to test propellers, motors and batteries under different loads. Testing includes charging and discharging many batteries (Lithium, Nickel Cadmium and Nickel-Metal-Hydride) under different loads to develop power curves for optimization of UAVs.

An important device being installed on the mini/micro UAVs is GPS. The range of applications of GPS increases as the size of the GPS decreases. Once a bulky, power hungry system, GPS circuitry has been reduced to the point where it can now be contained within a wristwatch. The smallest form-factor GPS circuitry currently available is the GPS2020 module.⁴ Although the GPS2020 contains all the required GPS functionality, it also requires external circuitry for power regulation, clock signaling for low-power modes, and RS-232, transceivers for serial communications with a navigation computer. The module outputs navigation and time data in an ASCII character-stream. It is up to the designer to put this information into a user-readable form, such as a map; thus, external software is required. This paper will also present the design and use of the circuitry and software external to the GPS2020 module, as well as ideas fundamental to the operation of GPS on these micro-air vehicles for swarming.

Fabrication of Test Bed

NASA Langley researchers are constantly working to develop stronger, lighter, more durable materials that can enhance earthbound flight and withstand the harsh conditions of space. Discoveries such as new adhesives, ceramics, plastics, and metal alloys will not only be

used in current and future aircraft and spacecraft, but some of these materials have a direct impact on our every-day lives. Research to improve the design of composite structures is continuing in manufacturing, analysis, and testing. Manufacturing efforts include finding new ways to position fibers to minimize discontinuities and interruptions in load paths, and to minimize failures due to minor damage or delaminations.⁵ Experience in lightweight and high-strength composite fabrication methods has been incorporated into the development of a test bed. Here is a brief description of fabrication methods.

Molds

The molds were cut with state-of-the-art CNC machining and tooling. The mold halves were prepared to a gloss finish as shown in figure 1. At this point, reference lines were redefined or added and additional preparation began for composite lay-up. These preparations included a release system utilizing application of a high-grade wax, thin coats of PVA (Poly Vinyl Alcohol). The wax and PVA are alternately layered insuring that the skin structure will release freely and easily.

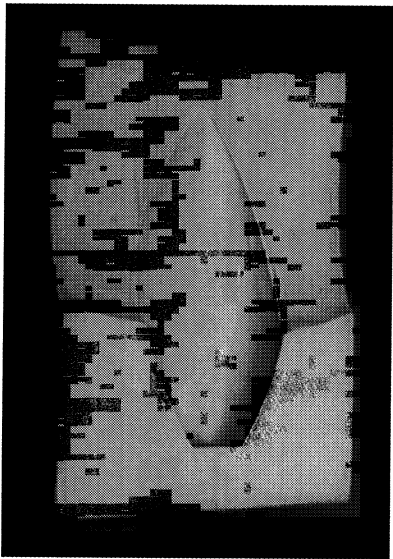


Figure 1. Gloss finish mold

Model

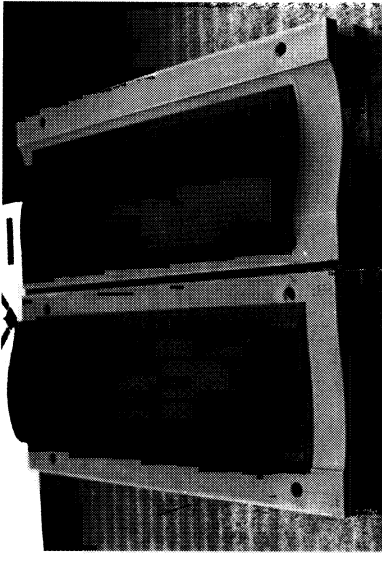
In a model, the skin represents the load bearing structure, yet has to be lightweight. To achieve this goal, several layers produced the desired results. The first layer (the exterior layer), is .004" bi-directional fiberglass. The second layer is .006" bi-directional graphite cloth for strength. Then a layer of AeroMat (.062"), which is a series of fibrous hexes held together and spaced apart via a thin film, was applied. This spacing results in an appearance that is a negative to the familiar honeycomb. The final layer (the interior layer) is .006" bi-directional graphite cloth. The resin system

used was West System Epoxy allowing for an overnight cure. The resin system was applied, and using a squeegee excess resin was removed, leaving behind enough resin to wet the laminates. When the final (interior) layer was added, the mold and laminates were "bagged" and a vacuum was applied to remove the air and apply pressure to the laminates for efficient molding of the skin.

Wing

The model has wings that are simple to detach, yet retain the correct alignment. This is accomplished with a two-pin system. A graphite tube was bonded to the lower wing skin, from wing root to wing tip, roughly along the 30% chord. A corresponding graphite tube had already been bonded in the fuselage. An aluminum pin was bonded into the wing's graphite tube and sets the dihedral. A sandwich structure (composed of 1/8" balsawood and .006" graphite on both sides) is used to complete the spar by filling in the gap from the tube to the upper wing skin.

Only one rib, made from 1/4" aircraft plywood, is at the root. At approximately 60% chord, a hole is drilled in the rib to accept a second pin. This aluminum pin is bonded in the fuselage rib and has a notch placed near its end. This notch just clears the inside of the wing's rib. A pivoting nylon catch swings and locks this pin in position, securing the wing firmly to the fuselage, preventing wing rotation and separation from the fuselage. The upper and lower wing halves were bonded together as shown in figure 2 using Scotch-Weld epoxy adhesive for a strong bond.



Fuselage
Figure 2. Strong Bond of upper and lower wing halves

The upper fuselage surface has a hatch (5" x 7") that is dually used to access the interior and to mount the

varying propulsion systems. Because of this three hatches were fabricated that were all rigid yet lightweight. The hatch, itself, was laid up in the upper fuselage mold using the following schedule. The first layer, .004" fiberglass, was cut to 6" x 8". The next ten layers of .006" graphite cloth were cut to 5" x 7", but were only 1/2" wide, leaving the center open. In addition, each alternating layer of the bi-directional cloth was cut at 45 degrees to increase stiffness. A piece of AeroMat was cut to fit the area formed by the 10 graphite layers. Finally, another piece of .006" graphite cloth was cut to 6" x 8" and applied over the previous layers. West System Epoxy Resin was used to bond the layers together under vacuum. After curing, the hatch was taken out, cut and finished to the final dimensions.

The upper fuselage mold was given the wax/PVA treatment in preparation for the skin lay up. The hatch was positioned and secured with a light application of Cynoacrylate Adhesive. The hatch was then given the wax/PVA treatment. After this, the fiberglass, graphite and AeroMat were applied and with the West System epoxy to form, under vacuum, the upper fuselage skin. With the hatch in place, a perfectly formed lip was created. After curing, the skin is removed, cleaned, and the hatch removed. At a later date, the hatch will be secured to the fuselage with two pins at the rear and with two sailplane latches at the front.

The lower fuselage skin is formed in the same manner as the other skins. Once made, the varying elements were added. Graphite tubes that secure the wing pins were bonded, the servo mounts were located and bonded in place, and ribs (1/4" aircraft plywood) were bonded at the sides where the wings would be placed. After these steps were done, the upper and lower fuselage skins were bonded together using Scotch-Weld 2216 epoxy adhesive as shown in figure 3.

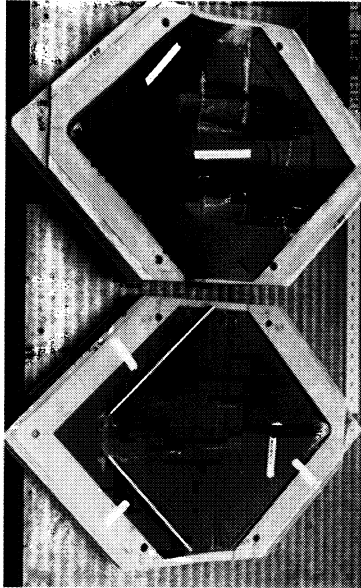


Figure 3. Upper and Lower fuselage

A picture of the complete model is shown in figure 4.

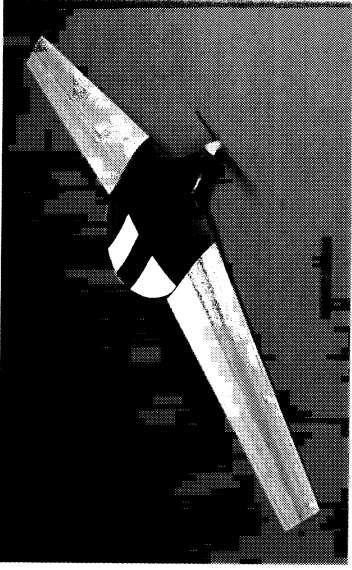


Figure 4. Complete Model

Table 1 presents the test bed parameters for the Langley MAV.

Table 1: Test Bed Parameters

Wing Span	59"
Type	Flying Wing
Control Surface	Elevon
Power	One Motor/Propeller
Nose	57g (2.04 oz.)
Center Section	258g (9.21 oz.)
Winglet ea.	25g (0.89 oz.)
Receiver	19g (0.68 oz.)
Servo ea.	21g (0.75 oz.)
Push Rods ea.	5.65g (0.20 oz.)
Push Rod Cover ea.	3.41g (0.12 oz.)
Motor	128.8 g (4.60 oz.)
Gear Box	44.8g (1.60 oz.)
Propeller/Spinner	30g (1.07 oz.)
Motor Controller	26g (0.93 oz.)
Battery	352g (12.57 oz.)
TOTAL	1281.72g (45.78 oz.)

Figure 5 shows the mass breakdown of the complete model.

Characterization Set-up of motors, batteries and propellers for use in Mini/ Micro Air Vehicles

The characterization set-up module as shown in figure 6, consists of a PC, a bench power supply, multifunction I/O card, GPIB card, tachometer, current sensor, air velocity transducer, thermocouple with conditioner, load cell, and all necessary interface hardware.

Mass Breakdown

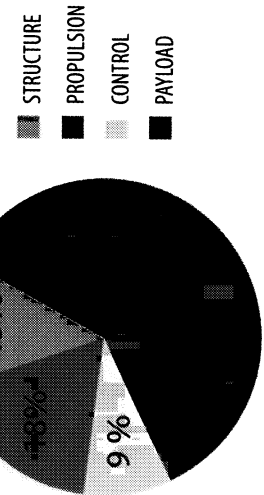


Figure 5. Mass Breakdown of complete model

The LabVIEW based software is used to control the DC voltage applied to the motor from the power supply. The software application continuously acquires 6 channels of data, calculates engineering units, updates on-screen dial readouts, displays accumulated data in on-screen strip charts, and saves the data to an ASCII spreadsheet file. The display and saved data include motor voltage, motor current, motor temperature, RPM, air velocity, thrust, calculated instantaneous power, calculated torque, and calculated accumulative watt-hours.

Motor/Propeller/Battery Characterization System

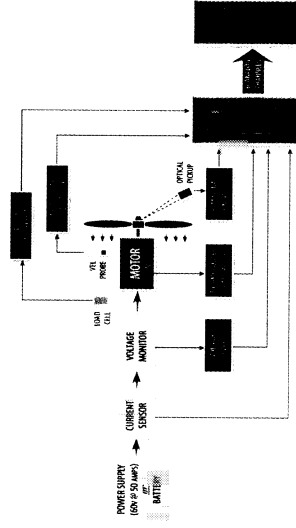


Figure 6. Characterization System Set-up

Figure 7 shows plots for power, current, and temperature vs. voltage for a motor. The current and power of the motor increases as expected corresponding to applied voltage. The figure shows a temperature increase as voltage is increased. The temperature increase is due to the increase in voltage and the load on the motor. The software application includes an alternate battery-life test-mode in which a battery

would be used instead of a DC power supply. In this mode, the software saves data at an interval specified by the user until the battery voltage drops to a preset level. The make and model of the load cell is selectable from a pull-down menu.

$$\text{Torque: } K_t = \frac{1352}{K_v} \quad (1)$$

$$\text{Torque (In-Oz)} = (K_t I_i) - (K_v I_o) \quad (2)$$

where I_i and I_o are in amperes.

Characterization of Motor (Power, Current and Temp.)

$$Cu\ Loss\ (watts) = I_i^2 R_M \quad (3)$$

where R_M is in Ohms

$$Fe\ Loss\ (Watts) = V_i I_0 \quad (4)$$

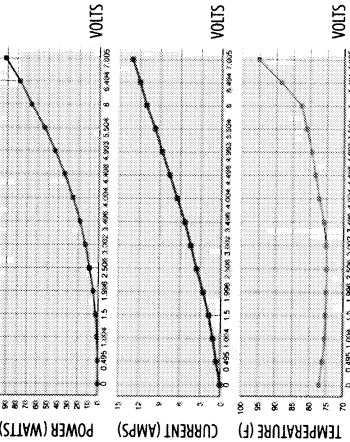
where V_i is in Volts.

$$\text{Efficiency (\%)} = \frac{100(I_i - I_0)(V_i - (I_i R_M))}{V_i I_i} \quad (5)$$

Measurement of Motor RPM

Figure 7. Power, Current and Temp. vs. Voltage plot for a motor

Motors for Micro-Air Vehicle are purchased on the ability to produce torque. A high torque low cost motor is preferred. All motors are limited by two factors; the thermal limit, and the RPM limit. The theoretical maximum power output of a motor is attained at the maximum RPM and maximum torque output. Figure 8 shows calculated torque, copper loss, iron loss, and motor efficiency. In addition, the torque curve is also affected by the motor load, prop, and gearbox.



Accurate RPM measurement is necessary to select the most efficient battery/motor/propeller and/or gearbox combination. Forward flight and hovering vehicles require quite different propulsion systems. Studying the effects on a motor's RPM based on varying combinations of the propulsion system's components is a valuable tool in configuring a successful flying vehicle. Additionally detecting a motor failure is also important. There are two methods to design Tachometer. First a wiring harness to connect to the real time system, the Hall effect sensor and magnets on the gears or motor fan. As the fan rotates, the Hall effect sensor detects the magnetic field and sends a signal to the board that counts the pulses. In the second method, an optics module is aimed to illuminate the spinner from the side. The light reflected off a white stripe on the spinner is detected each revolution by a photo sensor. Figure 8 shows RPM vs. volts. Ideally, this should be a straight line but because of iron and copper losses, this plot shows some hysteresis. The RPM is also affected by the load (prop diameter and pitch) and applied voltage.

Batteries

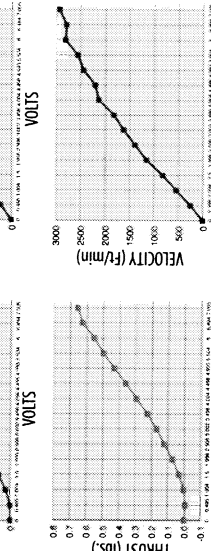


Figure 8. Torque, RPM, Thrust, and Velocity vs. Voltage for a motor

Fossil fuels have a higher energy density than batteries, but small internal combustion engines are noisy, require additional supplies for starting, and are inefficient. Solar cells cannot supply enough energy within the limited surface area of the mini/micro vehicles to sustain flight. At this stage, commercially available batteries are reliable and an inexpensive source of energy. Nickel-Cadmium (NiCd) and Nickel-Metal-Hydride (NiMH) batteries are used because of their high power density capabilities. The characterization

set-up is being used to characterize different types of batteries under different load conditions.

Table 2 presents a performance summary for the motor used in MAV

Table 2: Motor Details

Motor/Gearbox ratio	3.7:1
RPM/VOLT	2625
Current	28A
Propeller RPM	7800
Propeller Folding	10" x 8"
Static Thrust	50 oz.
Pitch Speed	61 mph
Max. Efficiency	88%

Air Velocity

TSI's Air Velocity Transducer measures velocities using thermal anemometry. This sensor provides flexibility with wide dynamic ranges for accurate measurements. The principle of operation is as follows.

An electric current is passed through a fine filament which is exposed to a cross flow. As the flow varies, the heat transfer from the filament varies. This in turn causes a variation in the heat balance of the filament. The filament is made from a material that possesses a temperature coefficient of resistance. The variation of resistance is monitored by various electronic methods and gives a signal corresponding to the variations in flow velocity or flow temperature. This method can be used for measuring instantaneous velocities and temperature. Air velocity was calculated and plotted as shown in figure 8. The non-smooth curve is due to turbulent airflow. The air speed is also affected by the propeller's design and the load on the propeller, which is due to the pitch and rpm.

Swarming

Swarming is a phenomenon whereby individual systems organized as networks use dispersed yet integrated operations. There are examples in nature, such as in beehives where a large group of individuals acts collectively to accomplish a task. In a similar fashion, fleets of vehicles, either airborne or ground based, as shown in figure 9, can be employed to accomplish large scale tasks. The starting point for research into this area is to review existing technologies that are needed to accomplish this task. For successful swarming, it is anticipated that following technologies are needed.

1. Sensor systems
2. GPS
3. Real-time communication between networking systems.
4. Superior situational awareness
5. Integration of command and control system.

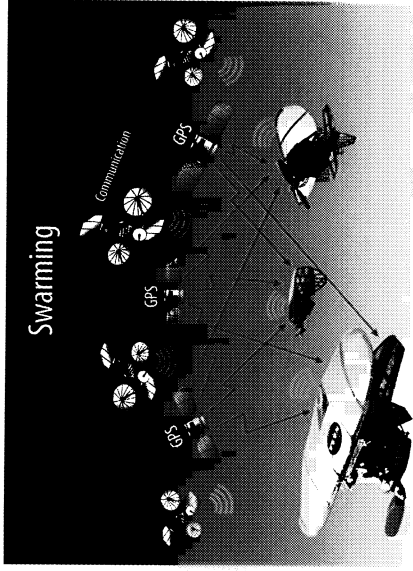


Figure 9. Swarming: individual systems organized as network

Individual units must communicate with high data throughput at all times, even in harsh environments. GPS-guidance and in-flight corrective maneuvering are important areas that must be investigated. The following experiment briefly describes how a GPS-synchronization test has been designed and set up in the lab.

Each GPS system as shown in figure 10 has three separate outputs: 1) a serial ASCII character stream containing position and timing information, 2) a one pulse-per-second (PPS) digital pulse, and 3) a digital waveform representing the GPS clock. For the synchronization experiment, the outputs of multiple GPS systems are simultaneously observed. Since one message sent through the serial data stream is relatively large, receiving clock information through this output is relatively slow. Additionally, the one PPS digital pulse is an inherently slow mechanism for extrapolating clock information. Thus, the only viable output from the GPS system that can be used for high frequency clocking is the digital GPS clock output. The synchronization experiment simultaneously observes the GPS clock outputs from several GPS systems, and measures the amount of synchronization/difference between the waveforms as they progress through time. That is, all GPS clocks from separate GPS systems should eventually synchronize to a common time base, within

some specific error range. The experiment attempts to determine this error range empirically.

GPS Synchronization Setup

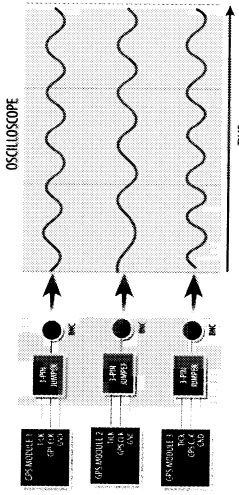


Figure 10. GPS Synchronization Setup

Electronic Subsystems including MEMS sensors

Semiconductor technology has developed considerably over the last several decades. The exponential growth has been achieved by a constant scaling down of integrated circuit size. Smaller feature sizes result in faster speed, and lower costs. Modern information systems are based on storage and retrieval; they compute, manipulate, and display data.

These systems are becoming part of our daily lives in cars, personal digital assistants, and palmtop systems. These systems must be able not only to compute but also to sense their physical environment and respond to it, e.g., inflating an air bag after sensing vibration. Such performance is achieved by Microelectromechanical Systems (MEMS) that consist of electrical and mechanical systems. MEMS devices are becoming part of our daily life from automobiles and communication equipment to aircrafts. These devices are critical to the operation and reliability of modern systems. Key features of MEMS devices are

- Miniature size
- Light weight
- High resonant frequency
- High operating frequencies and wide bandwidth
- Short thermal constant
- Localized distribution signal

One packaged MEMS sensor is shown in figure 11.

The sensor suite developed for our Micro-Air Vehicle consists of a pitot-static measurement system for determining air speed, an absolute pressure

measurement for determining altitude, magnetic sensor for direction measurement, and three orthogonal rate gyros to determine body angular rates. The suite of sensors is arranged and packaged to minimize the space required, and in a configuration that allows installation in the required flight test development vehicle. The output signals from the sensor suite are compatible with the data acquisition and feedback control system. The data acquisition system expects inputs to be analog signals between 0 to 5 volts. The sensor outputs are conditioned to provide maximum resolution of the measured parameters.

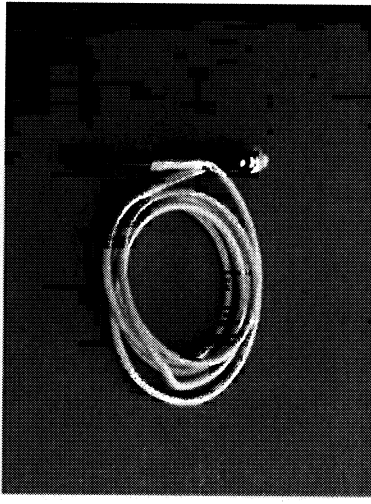


Figure 11. Packaged MEMS altitude sensor

It is important to note that if an electric motor is used to propel the vehicle, and the motor speed controller are in close proximity to the sensors, the effects of electromagnetic interference must be minimized.

Consideration is given to the current draw associated with the sensors and the effects of under and over voltage conditions. The sensor package can accommodate typical fluctuations in voltage and current, and minimize current draw.

Following is a brief description of individual sensors, GPS, data acquisition, and the feedback control system.

Gyros/Accelerometers

Piezoelectric Tokin gyros are used for angular rate sensing. They are miniature devices that provide high-speed response, and are magnetic-field resistant sensors. The offset and reference voltages of these gyros is around 1.3V. Each gyro is mounted orthogonal to the others so that all three axis of rotation can be measured.

The Crossbow sensor is a three-axis accelerometer. It does not measure angular change, but is used as a tilt sensor. Only two of the axes of rotation are measured;

The Z-axis is not connected. The accelerometer signal remains at a level corresponding to the effect of gravity in that direction. The voltage offset for the accelerometer is advertised to be at 2.5V, but is actually closer to 2.15V. The measured sensitivity is 360mV/g.

To test the accelerometer it was first mounted on a vertically revolving platform with the Y-axis under one g of acceleration, and the X-axis under no acceleration. The platform was then rotated, and at every 15 degrees, each axis output was sampled. At 90 degrees to the original configuration, the Y-axis is under no acceleration, and the X-axis is under one g of acceleration. At 180 degrees the X-axis is again under no acceleration, but the Y-axis is under one negative g of acceleration, the inverse of 0 degrees, while 270 degrees is the inverse of 90 degrees. Figure 12 shows plots of acceleration in the X and Y directions.

MEMS Accelerometer Data

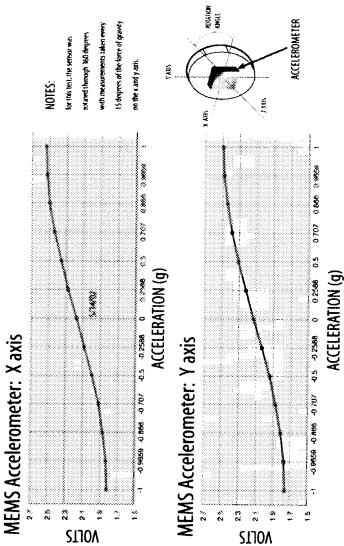


Figure 12. Output of MEMS accelerometers.

Altitude Measurement sensor

Piezoresistive silicon sensors can also be used for altitude measurement. These are monolithic silicon pressure sensors that provide an accurate, high-level analog output signal that is proportional to the applied pressure. Internal reliability and qualification tests use dry air as the pressure media. Silicon sensors are temperature dependent and have to be compensated in case of change in temperature. The altimeter used is an absolute sensor. Its output is connected to an operational amplifier. Two trimmers modify the gain and the offset of the amplifier circuit so that it can be calibrated. A Memson pressure controller was used to apply pressure to the sensor between the values of 14.8 psi and 13.0 psi. These values correspond to sea level and 3400 feet above sea level, respectively. If a different range of pressure is to be sensed, the offset/gain trimmers can be modified. The output from the sensor is inverted by the op-amp so that as pressure

increases, the voltage drops, until the lowest voltage is at sea level. Figure 13 shows the relationship between dropping pressure and rising voltage of the sensor.

MEMS Absolute Pressure Sensor For Altitude Measurement

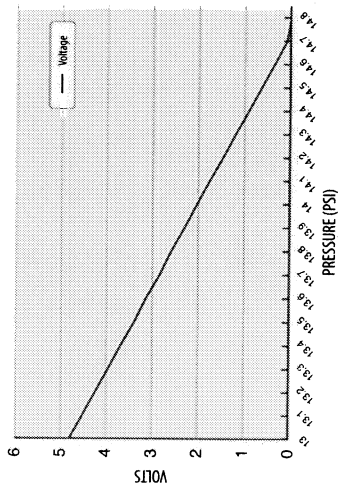


Figure 13. MEMS altimeter.

The MEMS altitude sensor is not accurate enough to safely work at or near ground level. If an airplane is attempting to land itself, a separate and more accurate sensor is required. To achieve this goal, an ultrasonic sonar transducer was used. This system is shown in figure 14.

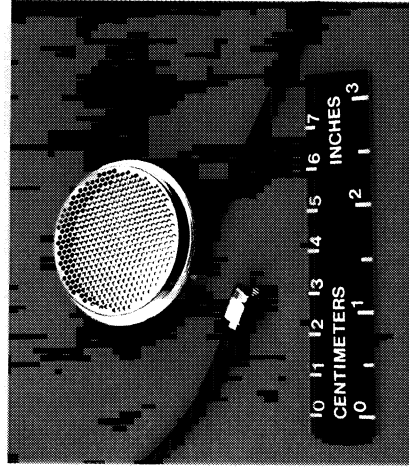


Figure 14. Ultrasonic Sonar Transducer

The sensor's accuracy and upper/lower bounds were tested using the MicroPilot MP2000, which is an auto-navigation and control system. This board sends all sensor data to a PC COM port that records all data. The transducer was mounted on a flat surface and placed at a few arbitrary known distances to verify that the measurement was correct. Since the published operating range of the sensor is between 6 inches and 15 feet (15-183 cm), these upper and lower bounds were next tested. The mounted transducer, shown in

figure 15, was pointed at the ground and lowered from 77 cm to 17 cm, in 5 cm increments. At each reading the distance was measured by hand and the sensor measurement was converted to centimeters so that the percent difference could be calculated. It was found that the difference between the hand measurements and

Ultrasonic Transducer Set-up

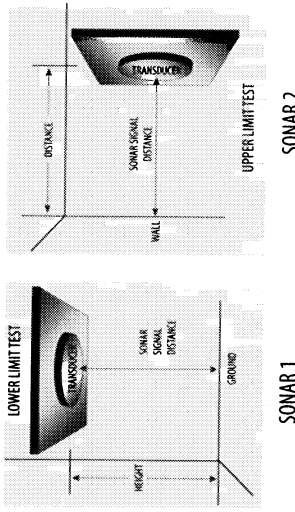


Figure 15. Ultrasonic Transducer Set-up

transducer measurements was approximately 1%, but this difference increased as the transducer approached 20 cm from the ground. From 20 cm (8 in.) and lower, the transducer reading stopped changing, and the percent difference became larger.

To test the upper operating range, the same procedure was used, but the mounted transducer was pointed towards a wall and the distance between them was increased from 9 feet to 14 feet (274 - 427 cm). The difference was still found to be around 1%, and increased as the distance between the wall and transducer increased. Figure 16 shows the difference between the transducer and hand measured distances.

Altitude Measurement by Ultrasonic Transducer

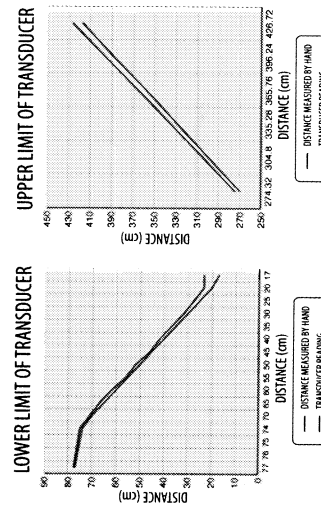


Figure 16: Comparison between Ultrasonic Transducer and hand measured distances

Air Speed

The differential air speed pressure sensor also has its output connected to an op-amp circuit. One trimmer is used to calibrate the signal gain. The silicon-based sensor has two ports, static and variable. The Mensor pressure controller was used to measure the outside air pressure and to apply a separate pressure to the static port. As the difference in pressure between the two ports increases, so does the output voltage. If both pressures are equal, the output is at its lowest, the offset voltage. The variable port during testing was simply exposed to the outside pressure, while a tube connected the static port to the controller. The controller applied a pressure from vacuum to 14.8 psi in increments of 0.1 psi. Figure 17 shows output voltage vs. difference in pressure.

MEMS Airspeed Sensor

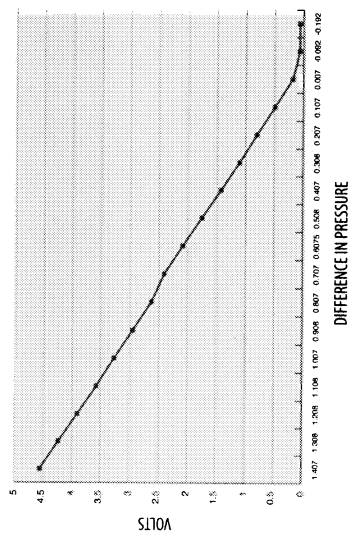


Figure 17. Output Voltage vs. difference in pressure
Three-axis Magnetic Sensor Hybrid

The navigation system requires some type of compass to determine heading direction. Using the earth's magnetic field, magnetoresistive sensors can resolve better than 0.1 degree of rotation. The earth's magnetic field intensity is about 0.5 to 0.6 gauss and can be approximated with the dipole model shown in figure 18. There are different types of compasses used for navigation systems: fluxgate, magnetoresistive, magnetooinductive, etc. Fluxgate compasses are commonly used for navigation systems, however they are bulky and has a slow response time.⁷ Magnetoresistive sensors provide a solid-state solution for navigation systems.

Humidity Sensors

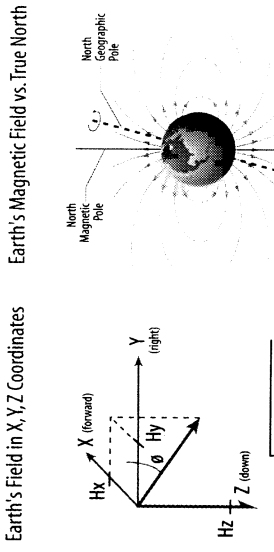


Figure 18: Earth's Dipole Model

Their high sensitivity and repeatability provide the best solution.

To measure the strength and direction of a magnetic field, Honeywell's 3-axis magnetic sensors are used. These transducers are sensitive to magnetic fields along the length, width, and height (X, Y, Z axes). Fields with intensities from 40 microgauss to ± 2 gauss can be detected. Unwanted noise is rejected using low-noise instrumentation amplifiers with 1 KHz low-pass filters.

Microphone

The silicon-based microphone used is shown in figure 19. This microphone has outstanding sensitivity and broadband response. The frequency response of this microphone is from 100 Hz through 60 KHz.

Individual Sensors & GPS for Unmanned Systems

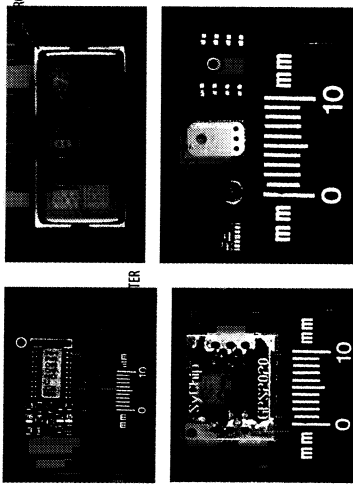


Figure 19. Silicon-based microphone

The MEMS humidity sensors have dimensions of 2mm x 2mm. The principle of MEMS sensors is: "A dab of polymer flexes a modified strain gauge in response to humidity changes."⁸ Data from these humidity sensors was taken at different temperatures and at different relative humidities. This data is shown in figure 20. As expected, MEMS humidity sensors are dependent upon temperature and have to be compensated.

IR-Camera

Non-cooled thermal imaging camera for unmanned vehicles has dimensions of 1.5" x 1.5" x 2" as shown in figure 21. It operates without cooling and at a frame rate of 30 Hz. The camera uses RS-232 interface.

MEMS Humidity Sensor

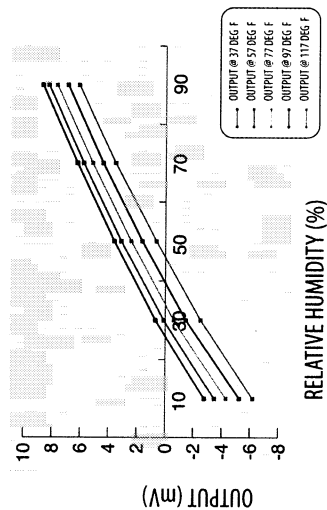


Figure 20. Characterization of MEMS humidity sensors.

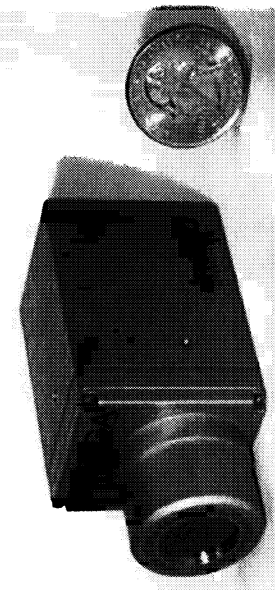


Figure 21. Non-cooled 1.5" x 1.5" x 2" Thermal Imaging Camera

An Autonomous Control System

There are few fully instrumented autonomous UAVs in use today. Most are much larger than the Micro/Mini

classification. In most cases, humans, through the use of ground-based commands, have real time vehicle control, of the UAV's flight parameters. As the supporting electronics technologies emerge, the human role will decrease to programmable onboard control systems.

For these micro-vehicles, lightweight material, sensors, and autonomous control is fundamental to the success of their long-duration flight. A Miniature Embedded Reconfigurable Computer and Logic (MERCAL) module, as shown in figure 22, was designed and fabricated by NASA/VCU that can provide significant hardware and software resources to meet the requirements of an autonomous control system.⁹ The major attraction of MERCAL is the reduction of the size, power and thermal requirements over existing logic control systems. This module can also be used for many of today's complex embedded applications. This is accomplished in the MERCAL module by combining a sub credit card size PC in a DIMM form factor with a XILINX Spartan II FPGA. The PC has the ability to download program files to the FPGA to configure it for different hardware functions and to transfer data to and from the FPGA via the PC's ISA bus during run time.

The MERCAL module combines, in a compact package, the computational power of a 133 MHz PC with up to 150,000 gate-equivalents of digital logic that can be reconfigured by software.

Control Board and Data-Logger for Unmanned Systems

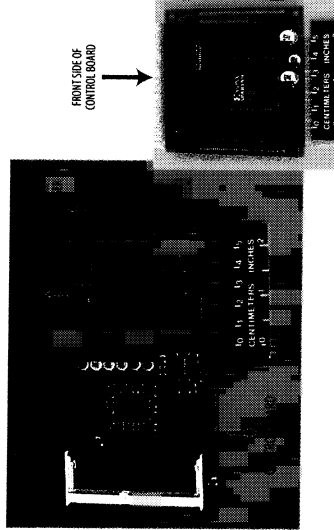


Figure 22. Control Board and Data Logger for Unmanned Systems

Conclusions

Micro/Mini air vehicles have been designed and fabricated as a test bed for a number of technologies that apply to aeronautics and space exploration. LaRC is a center of excellence in structures and materials, has an enabling fabrication lab, exceptional electrical and

mechanical engineering professionals, and a smart materials and sensors infrastructure. LaRC has multidisciplinary teams to address technology issues. The combination of capabilities and its multidisciplinary teams enable LaRC to meet project and custom needs. LaRC is a one-stop shop to carry an idea to reality.

Acknowledgements

The authors would like to thank our managers, Mr. Mark Hutchinson (ISDB/AAAC), Mr. Michael Mitchell (ISDB/AAAC), Dr. Robert McKinley (SAB/ASCAC), Mr. Pleasant W. Goode (SIB/ASC), Mr. Carl Voglewede (TD&IB/SEC), Mr. Tom J. Burns (TD&IB/SEC), Mr. M.E. Tall (TD&IB), and our colleagues Raymond V. Meyer (NCI/ASC), Ernest C. Burt (SEC), Dr. Martin R. Waszak (DCB/ASC), Dr. Robert G. Bryant (AMPB/SMC), Bob L. Myers(SEC), Bradley S. Sealey (ISDB/AAAC), Brian F. Beston (TCPD/NASA LaRC), Bill White (WYLE), and Louis M. Hartzheim (Raytheon) for their assistance in providing technical, graphics, design layout, hardware, and software support.

References

- ¹Grasmeyer J.M., Keenon Mathew T., "Development of the Black Widow Micro Air Vehicle" AIAA-2001-0127.
- ²H. Helvajin, "Microengineering Technology for Space Systems" The Aerospace Press, Monograph 97-02.
- ³"Proceedings of the Workshop on Microtechnologies and Applications to Space Systems" May 27-28, 1992 JPL Publications 93-8.
- ⁴"GPS2020 Module Application Note 1" SyChip Version 1.0 February 8, 2001.
- ⁵Siochi, Emilie J., Anders, John B. Jr., Cox, David E., Jegley, Dawn C., Fox, Robert L., and Katzberg, Stephen J., NASA/TM-2002-211445, Feb. 2002.
- ⁶Boucher, Robert J. "Electric Motor Handbook" ISBN 0-9644965-0-0.
- ⁷Caruso, Michael J., Honeywell Inc. "Applications of Magnetoresistive Sensors in Navigation Systems." Application Note.
- ⁸Ralph L. Fenner, 1973 "Use of Cellulose Crystalline Structures with solid state strain gauges for humidity and moisture measurement" ISA ASI 73249 1973, pp 251-252.
- ⁹Tucker, Jerry H., Klenke, Robert H. "VCU Department of Electrical Engineering, and Shams, Qamar A. (NASA Langley Research Center). "An Embedded Configurable Computer Module." Paper being submitted to IEEE Journal.

